

Underwater Carpet Cloak for Broadband and Wide-Angle Acoustic Camouflage Based on Three-Component Metafluid


Ping Zhou,^{1,2} Han Jia^{2,3,*}, Yafeng Bi,¹ Bin Liao,⁴ Yuzhen Yang,¹ Kaiqi Yan,⁴ Jingjie Zhang,⁴ and Jun Yang^{1,2,†}

¹Key Laboratory of Noise and Vibration Research, Institute of Acoustics, Chinese Academy of Sciences, Beijing 100190, People's Republic of China

²University of Chinese Academy of Sciences, Beijing 100049, People's Republic of China

³State Key Laboratory of Acoustics, Institute of Acoustics, Chinese Academy of Sciences, Beijing 100190, People's Republic of China

⁴Key Laboratory of Photochemical Conversion and Optoelectronic Materials, Technical Institute of Physics and Chemistry, Chinese Academy of Sciences, Beijing 100190, People's Republic of China

 (Received 19 March 2022; revised 3 May 2022; accepted 27 May 2022; published 20 July 2022)

Acoustic camouflage, which is realized by controlling wave propagation, has attracted great attention in recent years. Aided by a reflecting surface, the acoustic carpet cloak has become one of the most practically feasible invisibility devices and captured much experimental research enthusiasm. However, owing to the difficulty in the realization of ideal material parameters, the implemented underwater carpet cloaks could only work for a small incident angle. Here we design an underwater carpet cloak using a three-component metafluid composed of syntactic foam, steel, and water. The proposed syntactic foam, which is synthesized from epoxy resin and hollow glass microspheres, exhibits lower mass density and higher sound velocity relative to water. By periodically embedding the syntactic foam and steel rods in water, a carpet cloak is constructed and experimentally demonstrated in an anechoic water tank. Experimental results indicate that the designed carpet cloak works well under both normal and oblique incidences for broadband frequencies. The implementation of the designed underwater carpet cloak paves the way for future applications. Moreover, the introduction of syntactic foam in the design of the carpet cloak provides an extra degree of freedom for the acoustic parameter regulation of the metafluid in underwater acoustic devices.

DOI: [10.1103/PhysRevApplied.18.014050](https://doi.org/10.1103/PhysRevApplied.18.014050)

I. INTRODUCTION

Acoustic metamaterials have aroused great research enthusiasm because of their extraordinary ability to manipulate acoustic wave propagation at will. In recent years, a series of interesting acoustic phenomena have been realized with acoustic metamaterials, including negative refraction [1–3], and super-resolution focusing and imaging [4–6]. One of the most intriguing examples is acoustic invisibility technology [7–26], which can make a target acoustically undetectable. An acoustic carpet cloak [12,16–21,24], which conceals the target by mimicking the reflecting plane, has been recognized as one of the most practically feasible acoustic invisibility devices so far. There are two coordinate transformation methods to design the acoustic carpet cloak: quasiconformal transformation [24] and linear transformation [16–21]. The quasiconformal transformation results in a huge volume

and inhomogeneous parameters that are difficult to realize. By comparison, the linear transformation is favored more for the homogeneous parameters, simple design, and facile fabrication, which allow for huge application potential.

An ideal carpet cloak based on linear transformation requires anisotropic sound velocities and matched impedance. It is still challenging to exactly realize these parameters in experiment, especially in the underwater environment [11,19,20,23]. Previous works show that the sound velocities and impedance can be tailored by using a metafluid [8,10,12,16–24,27–29] consisting of discrete inclusions embedded in fluid. Brass and steel are usually chosen as solid inclusions embedded in water to form a two-component anisotropic metafluid [19,20]. However, this two-component metafluid achieves neither a sound velocity component higher than that of water nor the impedance matching with water, resulting in poor performance under a large-angle incoming wave and considerable additional scattering. Therefore, a component with lower mass density and higher sound velocity relative to

*hjia@mail.ioa.ac.cn

†jyang@mail.ioa.ac.cn

water is needed in the design of an underwater carpet cloak [16].

Here we synthesize a kind of syntactic foam and utilize it to design and fabricate an underwater acoustic carpet cloak, which can realize almost impedance-matched, broadband, wide-angle acoustic camouflage. The proposed syntactic foam, which is made of epoxy resin and hollow glass microspheres (HGMs), exhibits lower mass density and higher sound velocity relative to water. A three-component metafluid made of syntactic foam, steel, and water is designed to realize the anisotropic sound velocities and waterlike impedance. Then an underwater acoustic carpet cloak is designed based on the three-component metafluid. The measured acoustic pressure distributions under both normal and oblique incidences with different frequencies verify the excellent performance of the designed underwater carpet cloak.

II. RESULTS

A. Synthesis and characterization of syntactic foam

A bulk sample of syntactic foam made of epoxy resin and HGMs is shown in Fig. 1(a). By means of vacuum defoaming and molding technology, the syntactic foam can be made into arbitrary shapes according to different needs. The schematic diagram of the detailed synthesis process is shown in the Supplemental Material Fig. S2 [30]. A scanning electron microscope (SEM) image of the syntactic foam sample is shown in Fig. 1(b). The SEM image reveals that the HGMs are distributed evenly in epoxy resin and their diameters mostly fluctuate within a small range. These features ensure the homogenous mechanical properties of the syntactic foam. An enlarged view of the HGM is displayed in Fig. 1(c). The HGM exhibits a good spherical pattern and bonds perfectly with the epoxy resin, thus making it resistant against external stress. The inset in Fig. 1(c) shows a partial cross-section morphology of the HGM, which has a hollow structure and homogeneous wall thickness. Homogeneous and thin walls can effectively reduce the mass density of HGMs as well as guaranteeing a certain stress resistance. Generally, the acoustic properties of a material depend on its mass density and moduli. For the proposed syntactic foam, we can control its acoustic properties by adjusting the average geometric parameters and volume fraction of the HGMs.

To predict the acoustic parameters of syntactic foam, we employ the four-phase model [31–33] to calculate its mass density and bulk and shear moduli. As shown in the left panel of Fig. 1(d), the syntactic foam is modeled as four different phases, i.e., a three-layered spherical inclusion and a surrounding infinite medium with unknown effective properties (ρ^e , K^e , G^e). The three-layered composite sphere is comprised of an epoxy resin matrix shell, glass wall, and air core. The radii of the above three phases are indicated with a , b and c in Fig. 1(d). The radii of the

internal two-layered hollow sphere depend on the average wall thickness and average diameter of the HGMs. The matrix shell thickness is determined by the volume fraction of the HGMs. Each phase is homogeneous, linearly elastic, and isotropic. The composite sphere can be characterized by the same effective parameters as the surrounding infinite medium. Thus, the syntactic foam can be treated as a macroscopically homogeneous and isotropic medium as shown in the right panel of Fig. 1(d). The mass density, bulk modulus, and shear modulus of each phase in the composite sphere are known and denoted by ρ^i , K^i , G^i , where the superscript i is m for the matrix shell and w for the wall of the HGM. The air is ignored in the calculation because of its extremely small mass density. When the hydrostatic pressure and simple shear condition are applied at infinity, the average strain of the composite sphere should be the same as the strain of the effective medium. Combined with the boundary continuity condition at $r = a$, $r = b$, and $r = c$, we can calculate the strain of each phase, then the average strain of the composite sphere can be obtained. Thus, the effective bulk modulus (K^e) and shear modulus (G^e) of the syntactic foam can be expressed as follows:

$$K^e = \frac{K^w f (1 - (a/b)^3) \bar{\epsilon}_{ii}^w + K^m (1 - f) \bar{\epsilon}_{ii}^m}{\bar{\epsilon}_{ii}^{CS}}, \quad (1)$$

$$G^e = \frac{G^w f (1 - (a/b)^3) \bar{\epsilon}_{ij}^w + G^m (1 - f) \bar{\epsilon}_{ij}^m}{\bar{\epsilon}_{ij}^{CS}}, \quad (2)$$

where $\bar{\epsilon}_{ii}^w$, $\bar{\epsilon}_{ii}^m$, and $\bar{\epsilon}_{ii}^{CS}$ ($\bar{\epsilon}_{ij}^w$, $\bar{\epsilon}_{ij}^m$, and $\bar{\epsilon}_{ij}^{CS}$) are the compressive (shear) strain of the glass wall, epoxy resin matrix shell, and composite sphere, respectively. The subscripts i, j take the values 1, 2. More calculation details are shown in Appendix A. Additionally, the mass density of the syntactic foam is obtained through averaging the mass density of the components by volume

$$\rho^e = \left(1 - \left(\frac{b}{c}\right)^3\right) \rho^m + \left(\left(\frac{b}{c}\right)^3 - \left(\frac{a}{c}\right)^3\right) \rho^w, \quad (3)$$

where ρ^m and ρ^w refer to the mass density of the epoxy resin matrix shell and the glass wall, respectively. Therefore, the sound velocities of the syntactic foam, which can reflect the acoustic properties more directly, can be expressed as follows:

$$c_L = \sqrt{\frac{3K^e + 4G^e}{\rho^e}}, \quad (4)$$

$$c_T = \sqrt{\frac{G^e}{\rho^e}}, \quad (5)$$

where c_L and c_T are the sound velocities for longitudinal wave and transverse wave, respectively.

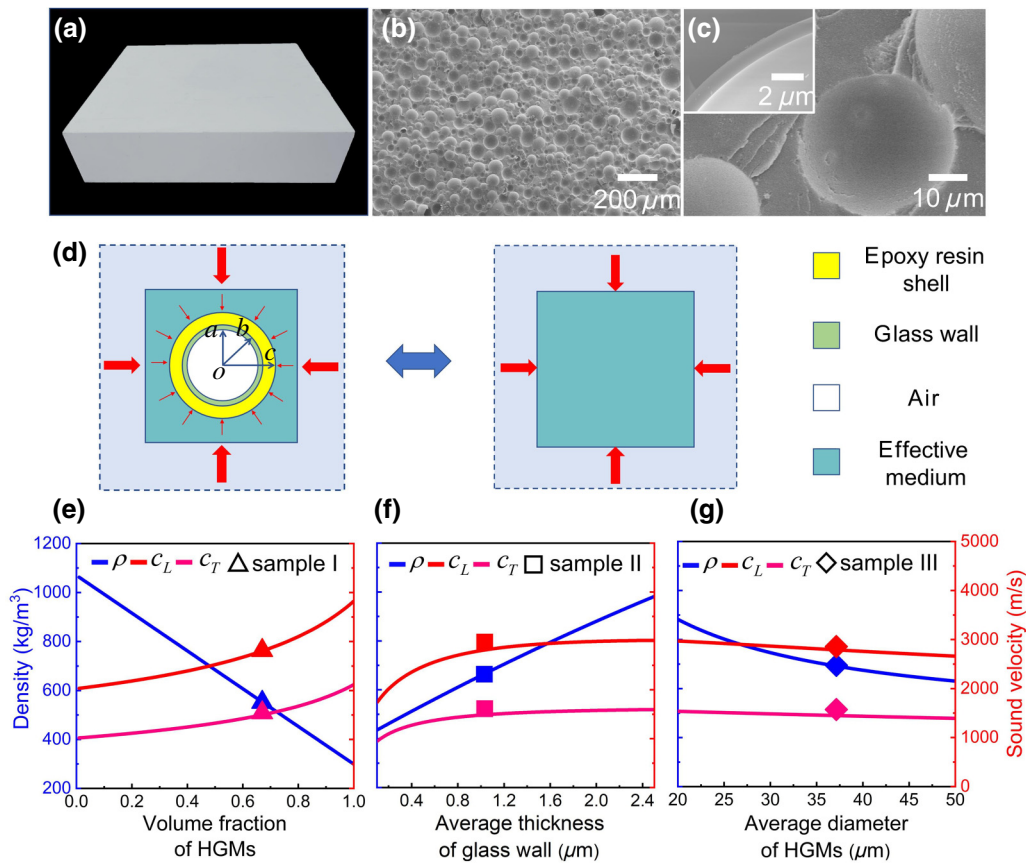


FIG. 1. Characterization of the syntactic foam. (a) Photo of a bulk sample. (b) SEM image of the syntactic foam showing the distribution of HGMs in epoxy resin matrix. (c) The morphology of the HGM and a partial enlarged view of cross-section morphology of the HGM shown in inset. (d) Left panel: the four-phase model is made of an infinite effective medium (light blue area), epoxy resin shell (yellow area), glass wall (light green area), and air (white area). The red arrows indicate the applied external force. The right panel: the macroscopically homogeneous effective medium. (e)–(g) The mass density (blue line) and sound velocity (red line for longitudinal wave, magenta line for transverse wave) of syntactic foam varying with the volume fraction of HGMs (e), average thickness of glass wall (f), and the average diameters of HGMs (g). The symbols mark the corresponding measurement values of the samples.

Through Eqs. (3)–(5), the acoustic parameters of syntactic foam with varying volume fraction and average geometric parameters of HGMs can be calculated conveniently. Figure 1(e) shows the mass density (blue curve) and sound velocities (red curve for longitudinal wave, magenta curve for transverse wave) for different volume fractions of HGMs. When the volume fraction is 0, the mass density is 1062 kg/m³, the sound velocities are 2045 m/s for longitudinal waves and 1031 m/s for transverse waves, which are exactly the acoustic parameters of the epoxy resin matrix. As the volume fraction increases, the syntactic foam can achieve lower mass density and higher sound velocities over a wide range. When the volume fraction is fixed, the average geometric dimensions of HGMs can also greatly affect the acoustic parameters of syntactic foam. It can be seen from the calculation results in Figs. 1(f) and 1(g) that thinner wall thickness and larger average diameter lead to lower mass density and

lower sound velocities. Accordingly, we fabricate three samples with different parameters. The three samples are denoted number I, II, and III. More information about the raw materials and acoustic parameters of the three samples is presented in the Supplemental Material Tables S1–S6 [30]. The corresponding acoustic parameters of the three samples are measured and labeled with symbols in Figs. 1(e)–1(g) for comparison. The results show that the measured values are in good agreement with the theoretical prediction. The measurement method for sound velocities is shown in the Supplemental Material Fig. S3 [30].

It can be observed from these results that the proposed syntactic foam presents lower mass density and higher sound velocities relative to water, and these acoustic parameters can be tuned in a wide range by adjusting the volume fraction and the geometric dimensions of the HGMs. The acoustic parameters of syntactic foam can exactly meet the demand for an

impedance-matched metafluid in the design of an underwater carpet cloak.

B. Design of the underwater acoustic carpet cloak

Here we use the syntactic foam and steel to form the metafluid and design an underwater acoustic carpet cloak. The proposed cloak is schematically shown in Fig. 2(a). The white triangle area on the reflecting surface is hidden space, whose half width is $n = 70.5$ cm, and height is $m = 10.1$ cm. The blue area indicating the carpet cloak, whose height is $h = 50$ cm, can conceal the hidden space by mimicking the reflection acoustic field of a reflecting plane. The required material parameters of the carpet cloak are calculated by transformation acoustics. The obtained mass density and bulk modulus are expressed as $\rho = \det(A)(A^{-1})^T(A^{-1})\rho_0$, $K = \det(A)K_0$, where $\rho_0 = 1000$ kg/m³ and $K_0 = 2.19$ GPa are the parameters of water, and A is the Jacobian matrix of transformation between physical space and transformed space. It can be noted that the transformed mass density is indicated by a tensor, which means it is anisotropic. This anisotropic mass density can be diagonalized by rotating the coordinate axes anticlockwise with angle α and simply represented by the

components in the principal axes ρ_{11} , ρ_{22} . In Fig. 2(a), the rotated coordinate axes are marked by x_{11} and x_{22} , which are also the principal axes of the material. To exhibit the acoustic properties more intuitively, sound velocities in the principal axes required by the carpet cloak are calculated by $v_{ii} = \sqrt{K/\rho_{ii}}$. Finally, the calculated results are $v_{11} = 1.026v_0$ and $v_{22} = 0.778v_0$, where $v_0 = 1480$ m/s is the sound velocity of water. The required sound velocities are plotted in Fig. 2(b) with solid curves. The calculation details can be found in Appendix B.

To realize the required acoustic parameters, we design the unit cell of the metafluid and show it in the red dashed frame in Fig. 2(a). It is a 10.5-mm by 30-mm rectangular lattice, in which the size of steel strip is 2 mm by 29 mm and the size of syntactic foam square is 4 mm by 4 mm. The number I syntactic foam is used here and the steel is characterized by mass density of 7850 kg/m³, Young's modulus of 205 GPa, and Poisson's ratio of 0.28. The background fluid is water. Sound velocities of the designed metafluid in the principal axis are calculated by using the retrieval method [34]. The results are presented in Fig. 2(b) with symbols for comparison. It can be seen that the sound velocities in both principal axes match well with the required parameters in a broadband range. The

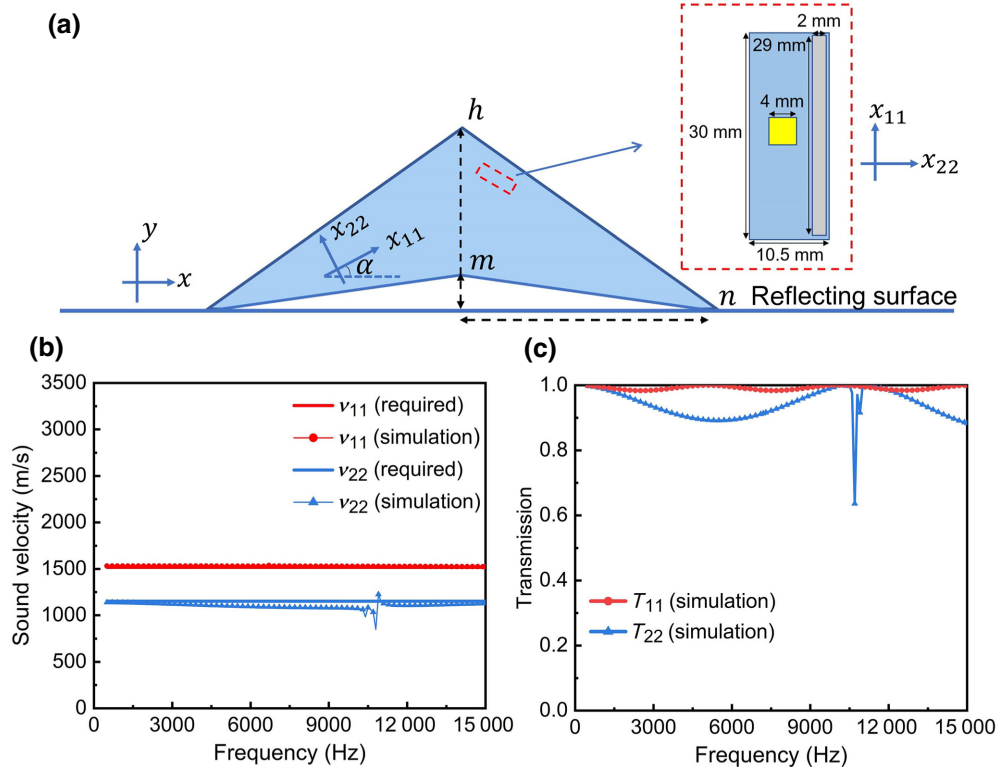


FIG. 2. The design of the underwater acoustic carpet cloak. (a) Schematics of the designed underwater carpet cloak mimicking the reflecting plane. x and y are the coordination axes of the physical space. x_{11} and x_{22} are the material principal axes of the required anisotropic parameters. $\alpha = 19.95^\circ$ is the rotation angle. The red dotted box displays the unit cell of the metafluid used to implement the carpet cloak. (b) The required and simulated sound velocities in the principal axes of the designed metafluid. (c) The simulated pressure transmission coefficient in the principal axes of the designed metafluid.

fluctuation near 11 kHz in the x_{22} direction stems from the narrow-band localized resonance of the steel strips. This fluctuation weakens rapidly with the direction change of the incident wave and has little effect on the broadband and wide-angle performance of the metafluid.

During the design process, we introduce a scale factor of $w^{-1} = 1.48$ in the transformation acoustics [30]. The introduced factor is so small that the designed metafluid can achieve almost perfect impedance matching with the background. We calculate the pressure transmission coefficients in the principal axes by placing five unit cells in a waveguide filled with water in the simulation. The calculated transmission coefficients in the two principal axes are labeled T_{11} and T_{22} and shown in Fig. 2(c). Although the transmission coefficients fluctuate in the broadband range because of Fabry-Perot resonance, the values in both principal axes are larger than 0.9 except near the localized resonant frequency of the steel strips. The high transmissions demonstrate the good impedance match between the metafluid and water.

C. Experimental demonstration of the underwater acoustic carpet cloak

We fabricate the sample using steel and syntactic foam rods. The shape of the cross section and the relative positions of rods are the same as the simulated ones. All these rods are inserted in two identical perforated plates to form a quasi-two-dimensional carpet cloak sample. The syntactic foam and steel rods arranged periodically are shown in the red dashed frame of Fig. 3(a). An air-filled triangular object sealed by thin steel plates is used as the target to be hidden. The photos of the entire sample equipment are shown in the Supplemental Material Fig. S4 [30].

The experiments are carried out in an anechoic water tank with a size of $50 \times 15 \times 10$ m. The schematic diagram of the experimental setup in water is shown in Fig. 3(a). The carpet cloak is upside down and placed with the bottom boundary level with the water surface. The sound source is mounted below the sample. The rectangular area marked with a blue dotted line is the measurement area, which is 1300 mm wide and 600 mm high. The detailed relative positions of the carpet cloak, sound source, and measurement area are marked on the right. In the measurement, an omnidirectional cylindrical transducer (C-MARK GA500) is set as the sound source to emit short Gaussian pulses modulated by different sinusoidal signals (5–15 kHz with 1 kHz step). Two hydrophones (Type 8103, B&K) are used to measure the pressure field distribution of the measurement area: one is fixed near the sound source for time-domain alignment, the other moves in the measurement area for scanning. In the measurement, the distance between adjacent measuring points is 2 cm to guarantee that each wavelength contains at least five measuring points. The pressure field distributions in three cases are

measured: the reflecting plane (the water-air interface), the target, and the cloaked target.

We first place the sound source directly below the sample for normal incidence and set the center frequency of the emitting Gaussian pulse as 5 kHz. The simultaneous reflected pressure fields of these three cases are measured and displayed in Fig. 3(b). Three rows from top to bottom correspond to the reflecting plane, the target, and the cloaked target. It can be observed that the waveform reflected from the reflecting plane is uniform and continuous. When the triangular target is placed under the water surface, the reflected waveform presents a discontinuous distribution. The existence of the slope makes most of the acoustic waves scatter to the side areas, thereby resulting in a shadow area in the middle region. After the target is covered with the carpet cloak, the shadow area is repaired and the scattered pressure field becomes as continuous and uniform as that of the reflecting plane.

Owing to the good match of sound velocities and impedance, the proposed carpet cloak can still maintain a good stealth performance when impinged upon by an incident wave at a large angle. In the experiment, we shift the sound source 3000 mm to the left and make the incident acoustic wave hit the sample at 45° . The instantaneous reflected pressure fields of the three cases at 5 kHz are displayed in Fig. 3(c). The protrusion and sharp edges of the target make its reflected pressure field discontinuous and locally concentrated. After the target is covered with the carpet cloak, the reflected pressure distribution characteristics of the target are completely eliminated. The phase and amplitude of the reflected wave from the cloaked target are extremely close to those of the reflecting plane, which indicates that the carpet cloak works well at a large incident angle. To show the broadband effectiveness of the carpet cloak, we also conduct the measurements at different frequencies. The measured pressure fields at 10 kHz and 12 kHz and the corresponding numerical simulations are shown in the Supplemental Material Figs. S5–S8 [30]. The dynamic videos of measured pressure field distributions under 45° incidence at 5 and 10 kHz are shown in the Supplemental Material Movies S1–S6 [30]. It is worth noting that the inherent loss in the syntactic foam hardly affects the cloaking performance of the carpet cloak for the small viscosity of the matrix in the syntactic foam and the low operating frequencies. See the detailed analysis and simulation in Note 1 [30].

To quantitatively show the performance of the carpet cloak, we extract the time-domain reflected signals at three special positions. These three positions are labeled A (0, 1900), B (60, 1900), C (90, 1900) in Fig. 3(a), corresponding to different characteristics of the reflected pressure field for the target under 45° incidence. The reflected signals at 10 kHz from the reflecting plane (black line), the target (blue line), and the cloaked target (red line) are plotted in Fig. 4(a). Compared with the reflected signals from

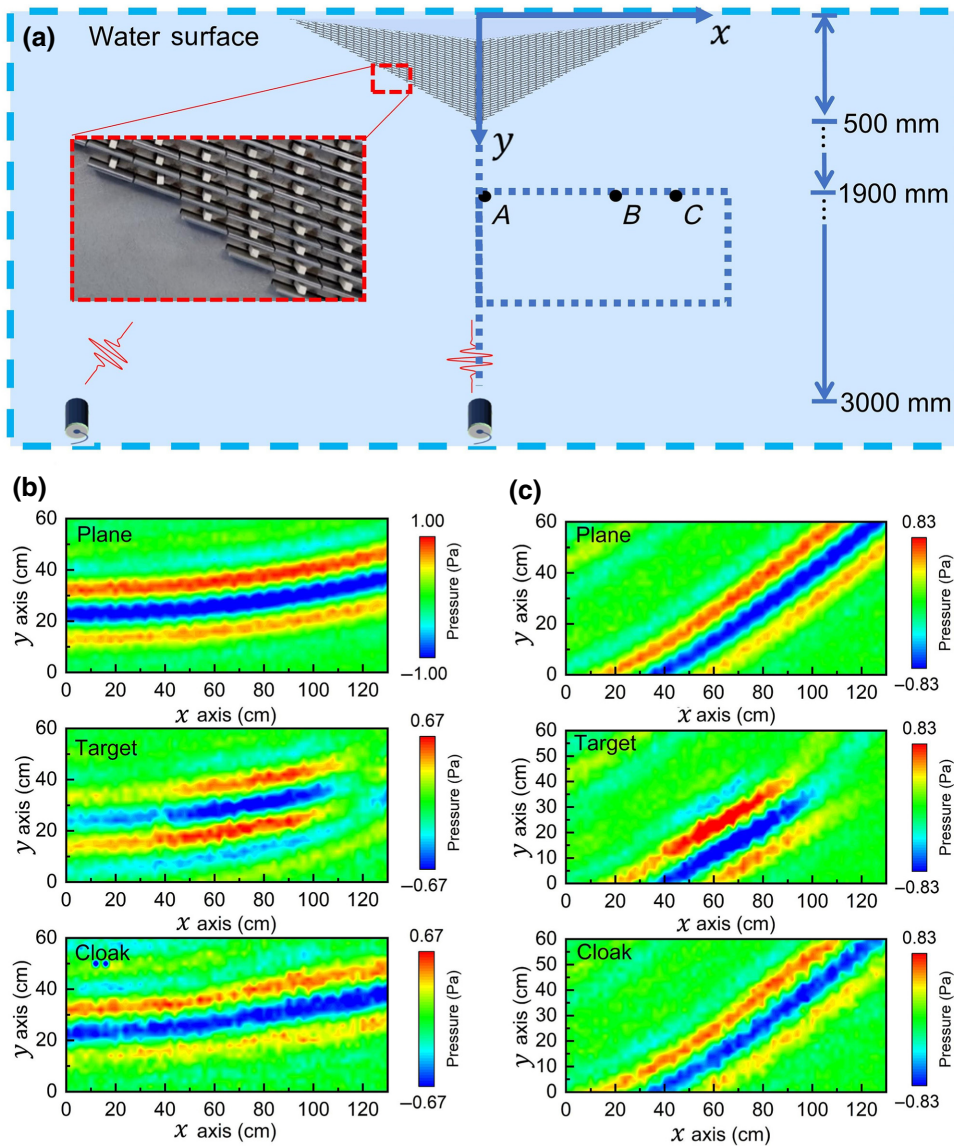


FIG. 3. Experimental demonstration of the underwater acoustic carpet cloak. (a) Schematics of the experimental setup. The photo of partial sample is shown in the red dashed frame. The relative positions of sound source (the middle one for normal incidence, the left one for oblique incidence), measurement area (blue dotted frame), and the carpet cloak are marked on the right. *A*, *B*, and *C* are three particular points to extract the time domain signals. (b), (c) The reflected pressure fields of the reflecting plane, target, and cloaked target for normal incidence (b) and 45° incidence (c) at 5 kHz.

the reflecting plane, there are always phase advances and amplitude fluctuations in the reflected signals from the target. The maximum phase advance occurring at point *C* is 180° while the amplitude ratio varies from 1.45 at point *B* to 0.25 at point *C*. It is obvious that the carpet cloak repairs the differences in both the amplitude and the phase between reflected signals from the target and the reflecting plane (phase difference within 30°, amplitude ratio above 0.74). The reflected signals from the reflecting plane and the cloaked target match well and their amplitudes hardly change with the positions, which proves that the impedance of the carpet cloak is close to that of water. The time-domain signal comparison results are consistent with the characteristics of the field distribution.

Finally, we use the cosine similarity index (C_{SI}) to comprehensively assess the performance of the carpet cloak.

The C_{SI} is defined as

$$C_{SI} = \frac{P^r \cdot P^0}{|P^r||P^0|} = \frac{\sum P_i^r P_i^0}{\sqrt{\sum (P_i^r)^2} \sqrt{\sum (P_i^0)^2}}, \quad (6)$$

where P^r represents the reference amplitude and denotes the reflected pressure amplitude matrix of the reflecting plane here, P^0 represents the reflected pressure amplitude matrices of the three measured cases, that is, the reflecting plane, the target, and the cloaked target, respectively. In Eq. (6), the closer the value of C_{SI} is to 1, the better the camouflage effect of the carpet cloak is. Figure 4(b) shows the C_{SI} in the three cases in the range of 5 to 15 kHz under 45° incidence. The C_{SI} between the cloaked target and the reflecting plane are above 0.85 while the C_{SI} between the target and the reflecting plane are below 0.6, which further

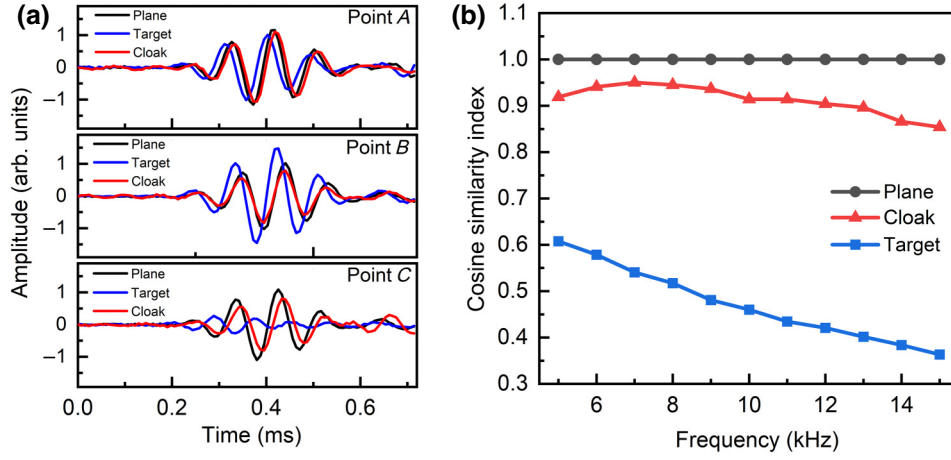


FIG. 4. Comprehensive experimental evaluation. (a) Extracted time-domain reflected signals at 10 kHz under 45° incidence. The locations of A , B , and C are marked in Fig. 3(a). Each panel contains the time-domain reflected signals of the reflecting plane (black curve), the target (blue curve), and the cloaked target (red curve). (b) The C_{SI} of the reflected pressure in the measurement area between the reflecting plane and the reflecting plane (black circles), the target (blue squares), and the cloaked target (red triangles) from 5 to 15 kHz.

verifies the effectiveness of the underwater acoustic carpet cloak within a broad frequency range. The slight deviation between the measured C_{SI} of the cloaked target and that of the reflecting plane originates from the fabrication error in sample size and additional scattering from the sample holder.

III. CONCLUSION

In conclusion, a broadband and wide-angle underwater acoustic carpet cloak is realized by utilizing syntactic foam and steel. The syntactic foam is synthesized from epoxy resin and HGMs. We use the four-phase model to accurately design and fabricate the syntactic foam with the required acoustic parameters. By organizing the syntactic foam and steel, we design a three-component metafluid that can achieve anisotropic sound velocities and impedance matching with water. Then the acoustic carpet cloak made of the proposed metafluid is designed and experimentally demonstrated. The measured reflected pressure fields under normal and oblique incidence verify that the designed carpet cloak can realize the acoustic camouflage for the wide-angle incoming wave. The impedance-matched effect is demonstrated via the consistency of phases and amplitudes of the reflected waves from the reflecting plane and the cloaked target. The subwavelength unit cell of the metafluid ensures the broadband effectiveness of the carpet cloak. In our work, the demonstration of an underwater acoustic carpet cloak based on the designed metafluid paves the way for practical engineering applications in underwater devices. Moreover, the realization of the impedance-matched underwater carpet cloak demonstrates that the proposed syntactic foam, as a synthetic material with adjustable components, can

provide a wide range of acoustic parameters and has great potential in the design of underwater acoustic devices. Nevertheless, more comprehensive and accurate underwater experiment is still a challenge in carpet cloak research. To further improve cloaking performance and promote its application, a more sophisticated fabrication method, such as three-dimensional printing, as well as more intelligent regulation and experimental design with the help of electromagnetism and machinery, may be helpful in future work.

ACKNOWLEDGMENTS

This work is supported by the Key-Area Research and Development Program of Guangdong Province (Grant No. 2020B010190002), the National Natural Science Foundations of China (Grants No. 11874383 and No. 12104480), and the IACAS Frontier Exploration Project (Grant No. QYTS202110).

APPENDIX A: ESTIMATES OF BULK AND SHEAR MODULI OF SYNTACTIC FOAM

For the four-phase model in Fig. 1, there are the following boundary conditions: the tractions vanishing at the boundary $r = a$, the tractions and displacements being continuous at the boundaries $r = b$ and $r = c$, and the strain field applied at infinity.

For the shear boundary conditions, the equation set is as follows:

$$\begin{aligned} 2I_1 - 8I_2 + C_1^w I_3 + C_3^w I_4 &= 0 \\ 40I_2 + C_2^w I_3 + C_4^w I_4 &= 0, \end{aligned} \quad (\text{A1})$$

$$\begin{aligned}
I_1 + \frac{a^5}{b^5}I_2 + \frac{b^2}{a^2}I_3 + \frac{a^3}{b^3}I_4 &= M_1 + \frac{a^5}{b^5}M_2 + \frac{b^2}{a^2}M_3 + \frac{a^3}{b^3}M_4 \\
-5\frac{a^5}{b^7}I_2 + \alpha_2^w \frac{1}{a^2}I_3 + (\alpha_{-3}^w - 5)\frac{a^3}{c^5}I_4 &= -5\frac{a^5}{b^7}M_2 + \alpha_2^m \frac{1}{a^2}M_3 + (\alpha_{-3}^m - 5)\frac{a^3}{b^5}M_4 \\
G^w \left(2I_1 - 8\frac{a^5}{b^5}I_2 + C_1^w \frac{b^2}{a^2}I_3 + C_3^w \frac{a^3}{b^3}I_4 \right) &= \\
G^m \left(2M_1 - 8\frac{a^5}{b^5}M_2 + C_1^m \frac{b^2}{a^2}M_3 + C_3^m \frac{a^3}{b^3}M_4 \right) & \\
G^w \left(40\frac{a^5}{b^7}I_2 + C_2^w \frac{1}{a^2}I_3 + C_4^w \frac{a^3}{b^5}I_4 \right) &= G^m \left(40\frac{a^5}{b^7}M_2 + C_2^m \frac{1}{a^2}M_3 + C_4^m \frac{a^3}{b^5}M_4 \right), \tag{A2}
\end{aligned}$$

$$\begin{aligned}
M_1 + \frac{a^5}{c^5}M_2 + \frac{c^2}{a^2}M_3 + \frac{a^3}{c^3}M_4 &= S_1 + \frac{a^5}{c^5}S_2 + \frac{a^3}{c^3}S_4 \\
-5\frac{a^5}{c^7}M_2 + \alpha_2^m \frac{1}{a^2}M_3 + (\alpha_{-3}^m - 5)\frac{a^3}{c^5}M_4 &= -5\frac{a^5}{c^7}S_2 + (\alpha_{-3}^e - 5)\frac{a^3}{c^5}S_4 \\
G^m \left(2M_1 - 8\frac{a^5}{c^5}M_2 + C_1^m \frac{c^2}{a^2}M_3 + C_3^m \frac{a^3}{c^3}M_4 \right) &= G^e \left(2S_1 - 8\frac{a^5}{c^5}S_2 + C_3^e \frac{a^3}{c^3}S_4 \right) \\
G^m \left(40\frac{a^5}{c^7}M_2 + C_2^m \frac{1}{a^2}M_3 + C_4^m \frac{a^3}{c^5}M_4 \right) &= G^e \left(40\frac{a^5}{c^7}S_2 + C_4^e \frac{a^3}{c^5}S_4 \right), \tag{A3}
\end{aligned}$$

$$S_1 = \gamma, \tag{A4}$$

where γ is the homogeneous shear strain field applied to the boundary of the four-phase model and G^w , G^m , G^e are the shear moduli of the glass wall, the matrix, and the surrounding medium, respectively. The coefficients α_2^i , α_{-3}^i , C_1^i , C_2^i , C_3^i , and C_4^i are the parameters associated with Poisson's ratio of each phase. The specific definitions can be found in Ref. [28]. The coefficients I_1, \dots, I_4 , M_1, \dots, M_4 , and S_1, \dots, S_4 are the unknown coefficients. The calculated shear strain of each phase and the average strain of the composite sphere are as follows:

$$\begin{aligned}
\bar{\varepsilon}_{ij}^w &= I_1 + \left(1 + \frac{1}{5}\alpha_2^w \right) \frac{b^5 - a^5}{a^2(b^3 - a^3)} I_3 \\
\bar{\varepsilon}_{ij}^m &= M_1 + \left(1 + \frac{1}{5}\alpha_2^m \right) \frac{c^5 - b^5}{a^2(c^3 - b^3)} M_3 \\
\bar{\varepsilon}_{ij}^{CS} &= M_1 + \left(1 + \frac{1}{5}\alpha_2^m \right) \frac{c^2}{a^2} M_3 + \frac{1}{5}\alpha_{-3}^m \frac{a^2}{c^3} M_4. \tag{A5}
\end{aligned}$$

Then substituting Eq. (A5) into Eq. (2), the shear moduli G^e can be calculated using the following quadratic

equations:

$$A \left(\frac{G^e}{G^m} \right)^2 + B \left(\frac{G^e}{G^m} \right) + C = 0, \tag{A6}$$

where the concrete expressions of coefficients A , B , and C can be found in Ref. [28].

For the compressive boundary conditions, the equation set is as follows:

$$3K^w J_1 - 4G^w J_2 = 0, \tag{A7}$$

$$\begin{aligned}
3K^w J_1 - 4G^w J_2 \frac{a^3}{b^3} &= 3K^m P_1 - 4G^m P_2 \frac{a^3}{b^3} \\
J_1 b + J_2 \frac{a^3}{b^2} &= P_1 b + P_2 \frac{a^3}{b^2}, \tag{A8}
\end{aligned}$$

$$\begin{aligned}
3K^m P_1 - 4G^m P_2 \frac{a^3}{c^3} &= 3K^e T_1 - 4G^e T_2 \frac{a^3}{c^3} \\
P_1 b + P_2 \frac{a^3}{c^2} &= T_1 b + T_2 \frac{a^3}{c^2}, \tag{A9}
\end{aligned}$$

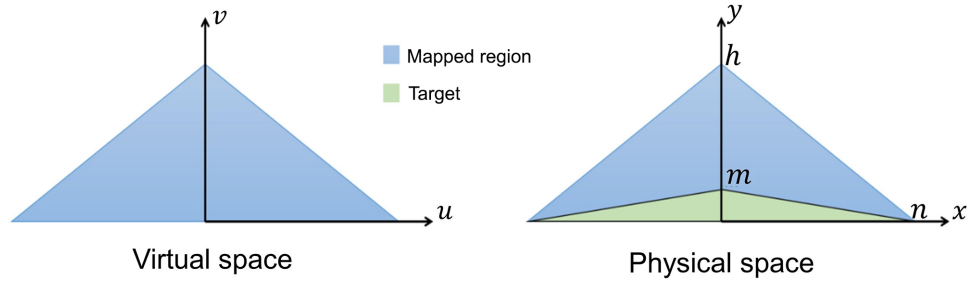


FIG. 5. A mapping between the virtual space and the physical space.

$$T_1 = \theta, \quad (\text{A10})$$

where θ is the homogeneous volumetric strain field applied to the boundary of the four-phase model and K^w , K^m , and K^e are the bulk moduli of the glass wall, the matrix, and the surrounding medium, respectively. J_1 , J_2 , P_1 , P_2 , T_1 , and T_2 are the unknown coefficients. The calculated compressive strain of each phase and the average strain of the composite sphere are as follows:

$$\begin{aligned} \bar{\epsilon}_{ii}^w &= 3J_1 \\ \bar{\epsilon}_{ii}^m &= 3P_1 \\ \bar{\epsilon}_{ii}^{CS} &= 3 \left(P_1 + P_2 \frac{a^3}{c^3} \right) \end{aligned} \quad (\text{A11})$$

Then substituting Eq. (A11) into Eq. (1) in the main text, the bulk modulus K^e can be obtained as follows:

$$K^e = K^m \frac{\delta(1 + (b^3/c^3)\beta) + k(1 - (b^3/c^3))\beta}{\delta(1 - (b^3/c^3)) + k(\beta + (b^3/c^3))}, \quad (\text{A12})$$

where $\beta = 4G^m/3K^m$, $\delta = (4G^w/3K^m)(1 - (a^3/b^3))$, $k = (4G^w/3K^w) + (a^3/b^3)$.

APPENDIX B: THE DESIGN OF THE CARPET CLOAK BASED ON TRANSFORMATION ACOUSTICS

The linear coordinate transformation method is used to design the carpet cloak. Figure 5 shows the virtual space (u, v) and the physical space (x, y) . A mapping to make the target in the physical space into a flat plane in the virtual space is established. The coordination transformation can be mathematically expressed as follows:

$$u = x, v = \frac{h}{h-m} \left(-m + \frac{m}{n} |x| + y \right), w = w_z z, \quad (\text{B1})$$

where m, n , and h are the geometric parameters in Fig. 5 and w_z is the scaling factor introduced to adjust the impedance mismatch between the background fluid and the transformation space. According to transformation acoustics theory, we can calculate the mass density and bulk

modulus of the cloak as

$$\begin{aligned} \bar{\rho} &= \det(A)(A^{-1})^T(A^{-1})\rho_0, \\ K &= \det(A)K_0 \end{aligned} \quad (\text{B2})$$

where ρ_0 is the mass density of the background fluid, K_0 is the bulk modulus of the background fluid, and A is the Jacobian of transformation $A = [\partial(u, v, w)/\partial(x, y, z)]^{-1}$.

In this work, the geometric dimensions are chosen as $m = 10.1$ cm, $n = 70.5$ cm, and $h = 50$ cm, and the background medium is chosen as water. The scaling factor is set as $w_z = 1$. Then the mass density tensor and bulk modulus can be calculated as

$$\begin{aligned} \bar{\rho} &= \begin{bmatrix} 0.824 & -0.18 & 0 \\ -0.18 & 1.253 & 0 \\ 0 & 0 & 0.798 \end{bmatrix} \rho_0 \\ K &= 0.798K_0. \end{aligned} \quad (\text{B3})$$

To obtain the required parameters in the material principal axes, the mass density tensor is diagonalized by rotating the coordinate axes through α . The rotation angle α can be calculated by

$$\alpha = \text{sign}(x) \arcsin \left(\frac{G}{\sqrt{G^2 - 1}} \right), \quad (\text{B4})$$

where $G = (n/h) \left(1 - ((h-m)/m) \left(F - 1 - \sqrt{F^2 - 1} \right) \right)$, $F = 1 + (m^2(n^2 + h^2))/(2n^2h(h-m))$. Here the rotation angle α is 19.95° . Then the diagonalized mass density is calculated as

$$\begin{aligned} \bar{\rho} &= \begin{bmatrix} 0.759 & 0 & 0 \\ 0 & 1.318 & 0 \\ 0 & 0 & 0.798 \end{bmatrix} \rho_0 \\ K &= 0.798K_0. \end{aligned} \quad (\text{B5})$$

To match the parameters of the designed metafluid, a small scale factor $w^{-1} = 1.48$ is introduced. Then the mass density components in the principal axes and bulk modulus are calculated as

$$\rho_{ii}^{pr} = w^{-1} \rho_{ii}, K_1 = w^{-1} K. \quad (\text{B6})$$

Intuitively, the required parameters can be expressed as sound velocities and impedance.

$$v_{ii}^{pr} = \sqrt{K_1 / \rho_{ii}^{pr}}, Z_{ii}^{pr} = \sqrt{K_1 \rho_{ii}^{pr}}, \quad (\text{B7})$$

It can be seen that the introduction of the scale factor does not change the distribution of the sound velocities, but makes the impedance of the carpet cloak $w^{-1} = 1.48$ times the required impedance, which matches well with the ideal impedance.

-
- [1] Y. Xie, B. I. Popa, L. Zigoneanu, and S. A. Cummer, Measurement of a Broadband Negative Index with Space-Coiling Acoustic Metamaterials, *Phys. Rev. Lett.* **110**, 175501 (2013).
- [2] H. He, C. Qiu, L. Ye, X. Cai, X. Fan, M. Ke, F. Zhang, and Z. Liu, Topological negative refraction of surface acoustic waves in a Weyl phononic crystal, *Nature* **560**, 61 (2018).
- [3] Y. Yang, Y. Ge, R. Li, X. Lin, D. Jia, Y. Guan, S. Yuan, H. Sun, Y. Chong, and B. Zhang, Demonstration of negative refraction induced by synthetic gauge fields, *Sci. Adv.* **7**, eabj2062 (2021).
- [4] J. Chen, J. Xiao, D. Lisevych, Amir Shakouri, and Zheng Fan, Deep-subwavelength control of acoustic waves in an ultra-compact metasurface lens, *Nat. Commun.* **9**, 4920 (2018).
- [5] Y. Shen, Y. Peng, F. Cai, K. Huang, D. Zhao, C. Qiu, H. Zheng, and X. Zhu, Ultrasonic super-oscillation wavepackets with an acoustic meta-lens, *Nat. Commun.* **10**, 3411 (2019).
- [6] T. Liu, F. Chen, S. Liang, H. Gao, and J. Zhu, Subwavelength Sound Focusing and Imaging via Gradient Metasurface-Enabled Spoof Surface Acoustic Wave Modulation, *Phys. Rev. Appl.* **11**, 034061 (2019).
- [7] H. Chen and C. T. Chan, Acoustic cloaking in three dimensions using acoustic metamaterials, *Appl. Phys. Lett.* **91**, 183518 (2007).
- [8] S. A. Cummer and D. Schurig, One path to acoustic cloaking, *New. J. Phys.* **9**, 45 (2007).
- [9] S. A. Cummer, B. I. Popa, D. Schurig, David R. Smith, John Pendry, Marco Rahm, and Anthony Starr, Scattering Theory Derivation of a 3D Acoustic Cloaking Shell, *Phys. Rev. Lett.* **100**, 024301 (2008).
- [10] D. Torrent and J. Sánchez-Dehesa, Acoustic cloaking in two dimensions: A feasible approach, *New. J. Phys.* **10**, 063015 (2008).
- [11] S. Zhang, C. Xia, and N. Fang, Broadband Acoustic Cloak for Ultrasound Waves, *Phys. Rev. Lett.* **106**, 024301 (2011).
- [12] W. Hu, Y. Fan, P. Ji, and J. Yang, An experimental acoustic cloak for generating virtual images, *J. Appl. Phys.* **113**, 024911 (2013).
- [13] T. S. Becker, D. J. van Manen, T. Haag, C. Bärlocher, X. Li, N. Börsing, A. Curtis, M. Serra-Garcia, and J. O. A. Robertsson, Broadband acoustic invisibility and illusions, *Sci. Adv.* **7**, eabi9627 (2021).
- [14] G. Yu, Y. Qiu, Y. Li, X. Wang, and N. Wang, Underwater Acoustic Stealth by a Broadband 2-Bit Coding Metasurface, *Phys. Rev. Appl.* **15**, 064064 (2021).
- [15] Z. Lu, L. Sanchis, J. Wen, L. Cai, Y. Bi, and J. Sánchez-Dehesa, Acoustic cloak based on Bézier scatterers, *Sci. Rep.* **8**, 12924 (2018).
- [16] B.-I. Popa and S. A. Cummer, Homogeneous and compact acoustic ground cloaks, *Phys. Rev. B* **83**, 224304 (2011).
- [17] B. I. Popa, L. Zigoneanu, and S. A. Cummer, Experimental Acoustic Ground Cloak in Air, *Phys. Rev. Lett.* **106**, 253901 (2011).
- [18] L. Zigoneanu, B. I. Popa, and S. A. Cummer, Three-dimensional broadband omnidirectional acoustic ground cloak, *Nat. Mater.* **13**, 352 (2014).
- [19] Y. Bi, H. Jia, W. Lu, P. Ji, and J. Yang, Design and demonstration of an underwater acoustic carpet cloak, *Sci. Rep.* **7**, 705 (2017).
- [20] Y. Bi, H. Jia, Z. Sun, Y. Yang, H. Zhao, and J. Yang, Experimental Demonstration of Three-Dimensional Broadband Underwater Acoustic Carpet Cloak, *Appl. Phys. Lett.* **112**, 223502 (2018).
- [21] P. A. Kerrian, A. D. Hanford, D. E. Capone, and B. S. Beck, Development of a perforated plate underwater acoustic ground cloak, *J. Acoust. Soc. Am.* **146**, 2303 (2019).
- [22] Y. Chen, X. Liu, and G. Hu, Latticed pentamode acoustic cloak, *Sci. Rep.* **5**, 15745 (2015).
- [23] Y. Chen, M. Zheng, X. Liu, Y. Bi, Z. Sun, P. Xiang, J. Yang, and G. Hu, Broadband solid cloak for underwater acoustics, *Phys. Rev. B* **95**, 180104 (2017).
- [24] Z. Sun, X. Sun, H. Jia, Y. Bi, and J. Yang, Quasi-isotropic underwater acoustic carpet cloak based on latticed pentamode metafluid, *Appl. Phys. Lett.* **114**, 094101 (2019).
- [25] X. Zhu, H. Ramezani, C. Shi, J. Zhu, and X. Zhang, PT-Symmetric Acoustics, *Phys. Rev. X* **4**, 031042 (2014).
- [26] X. Zhu, B. Liang, W. Kan, X. Zou, and J. Cheng, Acoustic Cloaking by a Superlens with Single-Negative Materials, *Phys. Rev. Lett.* **106**, 014301 (2011).
- [27] J. B. Pendry and J. Li, An acoustic metafluid: Realizing a broadband acoustic cloak, *New. J. Phys.* **10**, 115032 (2008).
- [28] B. I. Popa and S. A. Cummer, Design and characterization of broadband acoustic composite metamaterials, *Phys. Rev. B* **80**, 174303 (2009).
- [29] B. I. Popa, W. Wang, A. Konneker, S. A. Cummer, C. A. Rohde, T. P. Martin, G. J. Orris, and M. D. Guild, Anisotropic acoustic metafluid for underwater operation, *J. Acoust. Soc. Am.* **139**, 3325 (2016).
- [30] See Supplemental Materials of Underwater Carpet Cloak for Broadband and Wide-Angle Acoustic Camouflage Based on Three-Component Metafluid at <http://link.aps.org/supplemental/10.1103/PhysRevApplied.18.014050> for details of the preparation and measurement of syntactic foam, the characterization and analysis about loss in the syntactic foam, numerical simulations and more experimental results of the underwater carpet cloak at different frequencies and incident angles.
- [31] L. Bardella and F. Genna, On the elastic behavior of syntactic foams, *Int. J. Solids. Struct.* **38**, 7235 (2001).

- [32] E. Herve and O. Pellegrini, The elastic constants of a material containing holes, *Arch. Mech.* **47**, 223 (1995).
- [33] Z. Hashin, The elastic moduli of heterogeneous materials, *J. Appl. Mech.* **29**, 143 (1962).
- [34] V. Fokin, M. Ambati, C. Sun, and X. Zhang, Method for retrieving effective properties of locally resonant acoustic metamaterials, *Phys. Rev. B* **76**, 144302 (2007).